IEEE Access
Multidisciplinary ⋮ Rapid Review ⋮ Open Access Journal

Received June 17, 2021, accepted July 1, 2021, date of publication July 8, 2021, date of current version July 16, 2021.

Digital Object Identifier 10.1109/ACCESS.2021.3095553

Model Predictive Control With Triple Phase Shift Modulation for a Dual Active Bridge DC-DC Converter

SEEMA MIR AKBAR[1,2], AMMAR HASAN[1], ALAN J. WATSON[2], (Senior Member, IEEE), AND PAT WHEELER[2], (Fellow, IEEE)

[1]School of Electrical Engineering and Computer Science, National University of Sciences and Technology, Islamabad 44000, Pakistan
[2]Department of Electrical and Electronic Engineering, University of Nottingham, Nottingham NG7 2RD, U.K.

Corresponding author: Seema Mir Akbar (seema.akbar@nottingham.ac.uk)

ABSTRACT A fast dynamic response is one of the key demands for the dual active bridge (DAB) dc-dc converter to achieve a well-regulated output voltage over a wide range of operating conditions. Recently, model predictive control (MPC) has become a promising alternative to achieve fast dynamic response when compared to other classical converter control techniques. This paper presents an MPC based control approach augmented with a current stress optimized scheme based on triple phase shift (TPS) modulation to improve the dynamic performance and maintain a desired output voltage level without violating a minimum current stress constraint. A prediction model has been developed to accurately predict the dynamic behavior of the output voltage in the next horizon under the input voltage variations and load disturbances. As the model is developed using the TPS modulation thus inner phase shifts of the H-bridges as well as system's states are required to solve the formulated control problem. The inner phase shifts of the H-bridges are calculated using current stress optimized TPS scheme. Simulation and experimental results are provided to demonstrate the merits of the proposed control algorithm which includes a fast dynamic response without no overshoots in the output voltage, fixed switching frequency, low computational complexity and high degree of robustness.

INDEX TERMS Dual active bridge (DAB) dc-dc converter, triple phase shift (TPS), model predictive control(MPC), dynamic performance.

I. INTRODUCTION

Isolated dual active bridge (DAB) dc-dc converters, first proposed in [1], have received significant attention from the research community recently. They offer the advantages of high power density, bidirectional power flow, electrical isolation and the potential for soft switching. As such, they, or converters based on them, have been proposed for application areas such as renewable energy source interfaces, flexible AC transmission (FACTS), solid state transformers, drives systems and high voltage DC transmission (HVDC) [2]–[6].

The DAB dc-dc converter, shown in Fig. 1, consists of two H-bridges (HB) linked by a high frequency transformer. The transformer provides isolation and the leakage inductance is used as an energy storage and power transfer element. The power transfer and output voltage level of the converter can be controlled by single phase shift (SPS) modulation which modulates the phase shift ratio between the two H-bridges to obtain the required set points. SPS modulation is the most basic and simple technique which is widely used due to its easy implementation [29]. It can also achieve maximum power, however, this modulation scheme results in high ac current through the inductor, high reactive power and a loss of soft switching when the voltage gain deviates from one [29].

Various modulation techniques have been introduced to solve these problems; multiple phase shift modulation techniques introducing the inner phase ratios in each bridge of the DAB converter are among the most effective methods [29]. Based on the number of the phase shift ratios, these modulation methods can be classified as extended phase shift (EPS), dual phase shift (DPS) and triple phase shift (TPS). Compared with other modulation schemes, TPS utilizes all three available phase shift ratios and can maximize efficiency. It offers the advantages of reduced current stress and elimination of reactive power in the high frequency ac link, thus increasing

The associate editor coordinating the review of this manuscript and approving it for publication was Chi-Seng Lam.

the efficiency of the DAB dc-dc converter. This modulation scheme presents three degrees of freedom by allowing the control of the outer phase shift ratio between the two HBs as well as the inner phase shift ratios of HB1 and HB2. Based on the ranges of the three phase shifts, many distinct modes of operation can be obtained, each mode offering a different waveform and peak current for the same output voltage and transmission power. Many optimization control algorithms have been presented to find the optimal values of phase shift ratios, therefore minimizing current stress and the rms value of the inductor current [21]–[24].

The focus of the discussed modulation schemes is to the reduce current stress, eliminate reactive power and extend the soft switching operating range. However, in typical applications, such as those described above, dc-dc converter suffers from input source fluctuations, load transitions, and changes in output voltage demand. Thus, efficient control algorithms are also required for robust and fast dynamic performance of the DAB converter.

In recent years, model predictive control (MPC) has emerged as a promising solution to obtain fast dynamic response when compared to existing classical techniques used to control power converters [7], [8]. MPC explicitly utilizes a model of the system requiring control. The control action is calculated by minimizing a cost function that specifies the system behaviour. This cost function aims to minimize the error between predicted output and the reference using the system model. Since MPC can incorporate all the parameters/states of the system into the prediction model and thus can achieve a fast dynamic response whilst avoiding the complication of nested loops [8]. It can also be used efficiently in systems where multi-variable control is required. Furthermore, it allows the inclusion of non-linear effects and constraints in the control law in an uncomplicated manner [8], [27]. The performance of classical controllers such as proportional integral (PI) controller depends on the appropriate tuning of their parameters k_i and k_p, whereas in MPC schemes, there are no parameters to adjust [27]. Similarly, [37] has shown the relation between stability and the bandwidth of the PI controller, stating that increase in frequency can expand the stability range. Application of MPC based controller eliminates bandwidth limitation of the system [27]. Moreover, MPC eradicate the need of designing observers [32]. [35] and [36]. Observers are designed only to estimate the states that are otherwise not possible to measure easily [33]. However, MPC potentially suffers from computational burden owing to solving optimization problems in case of long prediction horizons. Different variants of MPC such as finite control set MPC and move blocking techniques have been presented to reduce the computational burden [9] and [10]. Thus, MPC based control algorithms have outperformed the traditional control techniques and currently the focus of the researcher is to develop the accurate model of the converter to be used in the optimization of the control process rather than proving the superiority of the MPC based control schemes [9], [14], [17], [33]–[36].

MPC algorithms have been extensively applied to different converter topologies to achieve fast dynamic performance [11]– [20] and [30]– [36], including active rectifiers [11], indirect matrix converters [12], three-level converters [13], voltage source inverters [14], and neutral-point-clamped converters [15]. MPC has also been implemented to optimize the dynamic performance of DAB dc-dc converters [16]–[20]. However, the existing applications of MPC in DAB converters are limited to the design of MPC based control for conventional modulation schemes such as SPS and DPS [16]–[20]. The control of the DAB converter operating under TPS is rarely addressed due to the complexity related to the development of the prediction model of the converter. Since there are three phase shifts as well as many different operating modes contributing to the difficulty of the control design [32]. An MPC based approach has been used in [32] to control the DAB converter operating under TPS and supplying power pulsed loads. The authors have proposed a finite control set MPC inspired approach by discretizing the outer phase shift. Thus an optimal phase shift needs to be searched in the discretized set of the phase shift values making the proposed control technique computationally troublesome.

This paper proposes an MPC technique with current stress optimization (CSO) based on the unified triple phase shift (UTPS) algorithm presented in [25] for a DAB dc-dc converter, to improve the dynamic performance and provide a well-regulated output voltage while realizing minimum current stress. In order to regulate the output voltage a control problem is defined which minimizes the error between the predicted output voltage and the desired voltage by controlling the phase shift between the H-bridges. A mathematical model is derived in this paper to predict the output voltage of the converter in the next horizon. As the model is developed using the TPS method the inner phase shifts of the H-bridges as well as system's states are required to solve the formulated control problem. The inner phase shifts of the H-bridges are calculated from expressions presented in [25] by utilizing karush-Kuhn-Tucker (KKT) equations to keep the current stress at a minimum. The optimal phase shift ratio results in fast dynamics in case of any disturbances in input, load or output response to the changing reference.

The rest of the paper is organized as follows: Section-II describes the TPS modulation scheme in detail. Section-III discusses the development of the prediction model for the output voltage of the converter. The MPC formulation is presented in Section-IV. Simulation results are presented in Section-V while the experimental results are presented in section-VI. Section-VII provides the conclusion of the paper.

II. UNIFIED TRIPLE PHASE SHIFT

A DAB dc-dc converter is shown in Fig. 1, and its general operating wave-forms under TPS control are shown in Fig. 2. V_{in} and V_0 are the dc voltages of the two HBs of the converter, V_{ab} and $\grave{V}_{cd}$ are the ac equivalent voltages of HBs on the input side. $\grave{V}_{cd}$ can be presented as the product of n and V_{cd},

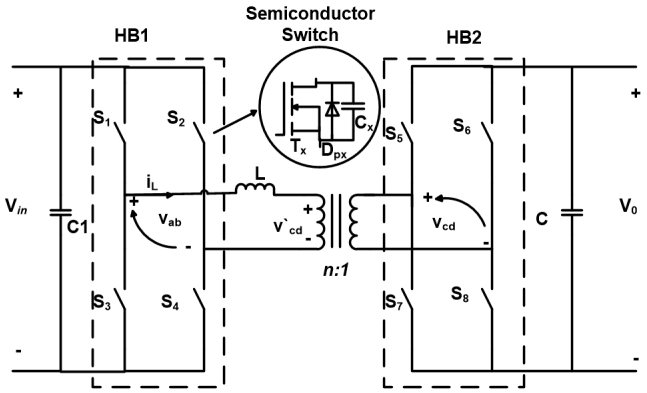

FIGURE 1. DAB DC-DC Converter.

where n denotes the primary to secondary turns ratio of the transformer. S_x denotes the semiconductor switch, which consists of the active switch T_x, anti-parallel diode D_{px}, and the junction capacitance C_x. L is the sum of any added series inductance and the leakage inductance of the transformer and i_L shows the inductor current. T_s is the switching period while the half switching period is given by T_{hs} and f is the switching frequency. The inner phase shifts ratios for HB1 and HB2 are defined as D_1 with range $0 \leq D_1 \leq 1$ and D_2 with range $0 \leq D_2 \leq 1$, respectively. The outer phase shift ratio between V_{ab} and $\grave{V}_{cd}$ is D_3 with the range $-1 \leq D_3 \leq 1$.

Moreover, D_f is defined as the phase shift ratio between the fundamental components of V_{ab} and $\grave{V}_{cd}$, which is related to other phase shifts given as:

$$D_f = D_3 + D_2/2 - D_1/2$$

As shown in Fig. 2, the switches on the same leg of the DAB always conducts in alternate half cycles such as S_1 and S_3, and S_2 and S_4 conduct in alternate half cycles. D_1 is the shift between the turning on of switch S_1 and S_2 as shown in Fig. 2. Switches S_1 and S_4 conducts in this duration while S_2 and S_3 are off resulting in voltage V_{ab}, which is equal to V_{in}, across the output of HB1. S_2 is turned on after D_1, thus S_1 and S_2 are conducting during this interval and no voltage appears across the output terminals of the HB1 until switch S_1 is turned off at the end of half cycle. S_2 and S_3 conduct from the start of half cycle until S_2 is turned off. At this interval the magnitude of V_{ab} is same as the input voltage but with negative direction.

Similarly, D_2 is the shift between the turning on of switch S_5 and S_6 of HB2 as shown in Fig. 2. Switches S_5 and S_8 conducts in this duration while S_6 and S_7 are turned off making V_{cd} equal to V_0. S_6 is turned on after D_2, thus S_5 and S_6 are conducting during this interval resulting on zero voltage until switch S_5 is turned off at the end of half cycle. S_6 and S_7 conduct from the start of the next half cycle until S_6 is turned off. At this interval the magnitude of V_{cd} is same as the output voltage but with negative direction.

D_3 is the phase shift between the first switch S_1 of HB1 and the first switch S_5 of HB2, which is same as the phase shift

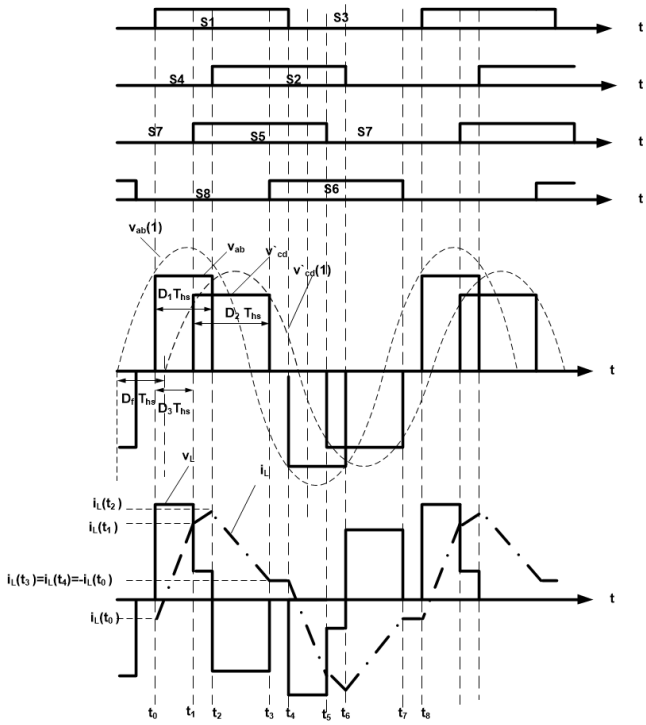

FIGURE 2. General operating waveforms of DAB with TPS.

TABLE 1. Mode Operational Constraints [25].

Switching Mode	Mode operational constraints
Mode I	$0 \leq D_f \leq \frac{D_2}{2} - \frac{D_1}{2}$
Mode II	$0 \leq D_f \leq \frac{D_1}{2} - \frac{D_2}{2}$
Mode III	$\left\lvert \frac{D_1}{2} - \frac{D_2}{2} \right\rvert \leq D_f \leq min\{\frac{D_1}{2} + \frac{D_2}{2}, 1 - \frac{D_1}{2} - \frac{D_2}{2}\}$
Mode IV	$1 - \frac{D_1}{2} - \frac{D_2}{2} \leq D_f \leq \frac{D_1}{2} + \frac{D_2}{2}$
Mode V	$\frac{D_1}{2} + \frac{D_2}{2} \leq D_f \leq 1 - \frac{D_1}{2} - \frac{D_2}{2}$

between the voltages V_{ab} and $\grave{V}_{cd}$. The inductor current slope changes based on the switching pattern as shown in the Fig. 2, and a switching period can be divided to small intervals depending on the shape of current waveform. The current equations for each interval are derived and discussed in detail in the subsequent section.

Expressions for the base values of power P_b and current I_b are defined in terms of input voltage V_{in}, series inductance L and switching period T_s as given by (1)

$$I_b = \frac{V_{in} T_s}{2\pi L}, \quad P_b = \frac{V_{in}^2 T_s}{2\pi L} \tag{1}$$

P_o is the required transmission power and P_{on} is the required transmission power normalized to base power given by (1). I_{pn} represents the current stress normalized to base current I_b given by (1).

Five distinct switching mode results based on the switching sequence of the two HBs for the operational constraints are presented in Table.1 [25]. The operating waveforms for all modes, which are used to derive the expressions for normalized transmission power and current stress, are given

TABLE 2. Optimal control parameters for selected switching modes [25].

Mode	Power range	Local optimal control parameters
Mode I	IA: $[0, \frac{(1-d)d^2\pi}{2}]$	$D_{1,opt} = \sqrt{\frac{2P_{on}}{(1-d)\pi}},\ \frac{D_{1,opt}}{d} \le D_{2,opt} \le 1,\ D_{f_opt} = \frac{\sqrt{2(1-d)\pi P_{on}}}{2d\pi}$
	IB: $[\frac{(1-d)d^2\pi}{2}, \frac{d\pi}{8}]$	$D_{1,opt} = \begin{cases} \frac{1}{2} - \frac{1}{2}\sqrt{\frac{d\pi-8P_{on}}{d\pi}}, 0 < d \le \frac{1}{2} \\ \frac{1}{2} + \frac{1}{2}\sqrt{\frac{d\pi-8P_{on}}{d\pi}}, \frac{1}{2} < d \le 0 \end{cases},\ D_{2,opt} = 1,\ D_{f,opt} = \begin{cases} \frac{1}{4} - \frac{1}{4}\sqrt{\frac{d\pi-8P_{on}}{d\pi}}, 0 < d \le \frac{1}{2} \\ \frac{1}{4} + \frac{1}{4}\sqrt{\frac{d\pi-8P_{on}}{d\pi}}, \frac{1}{2} < d \le 0 \end{cases}$
Mode II	IIA: $[0, \frac{d(1-d)\pi}{2(2-d)^2}]$	$D_{1,opt} = (2-d)\sqrt{\frac{2P_{on}}{d(1-d)\pi}},\ D_{2,opt} = \sqrt{\frac{2P_{on}}{d(1-d)\pi}},\ D_{f,opt} = \frac{\sqrt{2(1-d)\pi P_{on}}}{2d\pi}$
	IIB: $[\frac{d(1-d)\pi}{2(2-d)^2}, \frac{d\pi}{8}]$	$D_{1,opt} = 1,\ D_{2,opt} = \frac{1}{2} + \frac{1}{2}\sqrt{\frac{d\pi-8P_{on}}{d\pi}},\ D_{f,opt} = \frac{1}{4} + \frac{1}{4}\sqrt{\frac{d\pi-8P_{on}}{d\pi}}$
Mode III	IIIA: $[0, \frac{(1-d)d^2\pi}{2}]$	$D_{1,opt} = \sqrt{\frac{2P_{on}}{(1-d)\pi}},\ D_{2,opt} = \frac{1}{d}\sqrt{\frac{2P_{on}}{d(1-d)\pi}},\ D_{f_opt} = \frac{\sqrt{2(1-d)\pi P_{on}}}{2d\pi}$
	IIIB: $[\frac{(1-d)d^2\pi}{2}, \frac{d\pi}{6}]$	$D_{1,opt} = \frac{2}{3} - \frac{1}{3}\sqrt{\frac{(2-3d)^2(d\pi-6P_{on})}{(1-3d+3d^2)d\pi}},\ D_{2,opt} = \frac{2}{3} - \frac{1}{3(2-3d)}\sqrt{\frac{(2-3d)^2(d\pi-6P_{on})}{(1-3d+3d^2)d\pi}}$ $D_{f,opt} = \frac{1}{3} - \frac{1-3d}{6(2-3d)}\sqrt{\frac{(2-3d)^2(d\pi-6P_{on})}{(1-3d+3d^2)d\pi}},$
Mode IV	IVA: $[0, \frac{(1-d)d^2\pi}{2}]$	$D_{1,opt} = \begin{cases} \frac{1}{2} - \frac{1}{2}\sqrt{\frac{d\pi-8P_{on}}{d\pi}}, 0 < d \le \frac{1}{2} \\ \frac{1}{2} + \frac{1}{2}\sqrt{\frac{d\pi-8P_{on}}{d\pi}}, \frac{1}{2} < d \le 0 \end{cases},\ D_{2,opt} = 1,\ D_{f,opt} = \begin{cases} \frac{1}{4} - \frac{1}{4}\sqrt{\frac{d\pi-8P_{on}}{d\pi}}, 0 < d \le \frac{1}{2} \\ \frac{1}{4} + \frac{1}{4}\sqrt{\frac{d\pi-8P_{on}}{d\pi}}, \frac{1}{2} < d \le 0 \end{cases}$
	IVB: $[\frac{(1-d)d^2\pi}{2}, \frac{d\pi}{4}]$	$D_{1,opt} = 1 - (1-d)\sqrt{\frac{d\pi-4P_{on}}{(1-2d+2d^2)d\pi}},\ D_{2,opt} = 1,\ D_{f,opt} = \frac{1}{2} - \frac{1}{2}\sqrt{\frac{d(d\pi-4P_{on})}{(1-2d+2d^2)\pi}}$
Mode V	VA: $[0, \frac{d^2\pi}{2(1+d)^2}]$	$D_{1,opt} = \frac{\sqrt{2\pi P_{on}}}{\pi},\ D_{2,opt} = \frac{\sqrt{2\pi P_{on}}}{d\pi},\ D_{f,opt} = \frac{(1+d)\sqrt{2\pi P_{on}}}{2d\pi}$
	VB: $[\frac{d^2\pi}{2(1+d)^2}, \frac{d\pi}{8}]$	$D_{1,opt} = \frac{1}{2} - \frac{1}{2}\sqrt{\frac{d\pi-8P_{on}}{d\pi}},\ D_{2,opt} = \frac{1}{2} + \frac{1}{2}\sqrt{\frac{d\pi-8P_{on}}{d\pi}},\ D_{f,opt} = \frac{1}{2}$

in [25]. The Karush-Kuhn-Tucker (KKT) approach, which takes into account all the equality and inequality constraints in solving an optimization problem, has been used to find the optimized solution given by $X_* = (D_{f,opt}, D_{1,opt}, D_{2,opt})$ for minimum current stress. $D_{1,opt}, D_{2,opt}, D_{3,opt}$ and $D_{f,opt}$ represents optimal phase shifts. The boundary conditions of the optimal phase shifts result in two different transmission ranges: the lower transmission power range is identified as range-A and the higher transmission power range is referred to as range-B. The optimal phase shift values resulting in minimum current stress and the transmission power ranges arising from the optimal control parameters of each mode are given in the Table. 2. The optimal phase shifts depend on required normalized transmission power P_{on} and d where d is conversion ratio given below.

$$d = \frac{V_0}{V_{in}}$$

III. MATHEMATICAL MODELLING OF THE CONVERTER

Mode-III and mode-IV have been proven as the global optimal operating modes to obtain minimum current stress for low and high power ranges in [25]. This paper has focused only on mode-III; the same procedure can be followed for mode-IV and other modes. The inductor voltage and current waveform for mode-III are shown in Fig.2. Assuming that $V_{ab} > \grave{V}_{cd}$, inductor voltage V_L and current $i_L(t)$ are given by (2) and (3), respectively:

$$V_L = V_{ab} - \grave{V}_{cd} \tag{2}$$

$$i_L(t) = \frac{1}{L}\frac{V_L}{dt} \tag{3}$$

Only half of the sampling period t_0-t_4 is considered due to symmetry. There are four intervals t_0-t_1, t_1-t_2, t_2-t_3 and t_3-t_4 as shown in Fig.2. The inductor current at the start of the sampling period and at the end of each interval calculated using (3) are given by (4a)-(4e) [26].

$$i_L(t_0) = \frac{T_s n V_o}{4L}(D_2 - KD_1) \tag{4a}$$

$$i_L(t_1) = \frac{T_s n V_o}{4L}(D_2 - KD_1 + 2KD_3) \tag{4b}$$

$$i_L(t_2) = \frac{T_s n V_o}{4L}(D_2 + KD_1 - 2D_1 + 2D_3) \tag{4c}$$

$$i_L(t_3) = \frac{T_s n V_o}{4L}(KD_1 - D_2) \tag{4d}$$

$$i_L(t_4) = \frac{T_s n V_o}{4L}(KD_1 - D_2) \tag{4e}$$

where
$K = \frac{V_{ab}}{\grave{V}_{cd}}$, $V_{ab} = V_{in}$ and $\grave{V}_{cd} = nV_0$.

The average current for each interval can be calculated as given below [18]:

$$\bar{i}_L(t_1) = \frac{i(t_0) + i(t_1)}{2} \tag{5a}$$

$$\bar{i}_L(t_2) = \frac{i(t_1) + i(t_2)}{2} \tag{5b}$$

$$\bar{i}_L(t_3) = \frac{i(t_2) + i(t_3)}{2} \tag{5c}$$

$$\bar{i}_L(t_4) = \frac{i(t_3) + i(t_4)}{2} \tag{5d}$$

KCL is applied at the output node to find differential equation of the output voltage for each interval as follows:

$$C\frac{dV_0}{dt} = -i_0 \quad t \in \left[0, \frac{D_3 T_s}{2}\right] \tag{6a}$$

$$C\frac{dV_0}{dt} = \bar{i}_L(t_2) - i_0 \quad t \in \left[\frac{D_3 T_s}{2}, \frac{D_1 T_s}{2}\right] \tag{6b}$$

$$C\frac{dV_0}{dt} = \bar{i}_L(t_3) - i_0 \quad t \in \left[\frac{D_1T_s}{2}, \frac{(D_2+D_3)T_s}{2}\right] \tag{6c}$$

$$C\frac{dV_0}{dt} = -i_0 \quad t \in \left[\frac{(D_2+D_3)T_s}{2}, 1\right] \tag{6d}$$

where i_o is output current of the converter. Currents $\bar{i}_L(t_2)$ and $\bar{i}_L(t_3)$ calculated using (4) and (5) are presented

$$\bar{i}_L(t_2) = \frac{T_snV_o}{4L}(D_2 + KD_3 - D_1 + D_3) \tag{7}$$

$$\bar{i}_L(t_3) = \frac{T_snV_o}{4L}(KD_1 - D_1 + D_3) \tag{8}$$

The average differential output equation is given as:

$$C\frac{dV_0}{dt} = \frac{T_snV_o}{4L}(KD_3^2 + 2KD_3D_1 + KD_1D_2) - i_0 \tag{9}$$

Putting the value of K in (9) we get

$$C\frac{dV_0}{dt} = \frac{T_sV_{in}}{4L}(D_3^2 + 2D_3D_1 + D_1D_2) - i_0 \tag{10}$$

$$\frac{dV_0}{dt} = \frac{V_0(k+1) - V_0(k)}{t_{k+1} - t_k} \tag{11}$$

$$\frac{dV_0}{dt} = \frac{V_0(k+1) - V_0(k)}{T_s} \tag{12}$$

The Euler equation given in (11) and (12) is used to discretize (10) to find the predicted value for the output voltage at time (k+1). Thus, the output voltage for the next state can be predicted by:

$$V_0(k+1) = V_0(k) + \frac{V_{in}}{4Cf^2L}(D_3^2 + 2D_3D_1 + D_1D_2) - \frac{i_0}{fC} \tag{13}$$

IV. MPC FORMULATION

The MPC strategy involves the prediction of future outputs at each sampling instant, k, for a prediction horizon, N, using the prediction model presented in section III. The predicted outputs $\hat{V}(k+j/k)$ for $j = 1 \ldots N$ depend on the future control input signals $D_3(k+j/k)$ for $j = 0 \ldots N-1$, as shown in (14).

$$\hat{V}_0(k+1/k) = V_0(k) + \frac{V_{in}}{4Cf^2L}(D_3^2(k/k) + 2D_1D_3(k/k) + D_1D_2) - \frac{i_0}{fC} \tag{14}$$

The predicted output voltage and optimal phase shift $\overline{D\_3}$ which is the controlled input over the prediction horizon N can be defined in vector form as given in (15) and (16), respectively.

$$V = \left[\hat{V}_0(k+1/k)\ \hat{V}_0(k+2/k) \ldots \hat{V}_0(k+N/k)\right]^T \tag{15}$$

$$\overline{D\_3} = \left[D_3(k)\ D_3(k+1)\ \ldots\ D_3(k+N-1)\right]^T \tag{16}$$

To track the desired output voltage accurately and rapidly, a sequence of control input signals are calculated by minimizing a cost function defined over a prediction horizon N. The function to be optimized is a quadratic function that measures the difference of the predicted output voltage of the converter and a reference sequence on this horizon, subject to some constraints. The MPC control problem for DAB dc-dc converter with TPS can be formulated as follows.

$$\text{Cost function } J = \sum_{j=1}^{N}\left[\hat{V}_0(k+j/k) - V_0^{ref}(k+j)\right]^2$$

subject to constraints

$$\left\{D_1 - D_2 \le D_3 \le \min(D_1, 1-D_2) \quad \text{mode-III}\right. \tag{17}$$

The control objective is to compute the sequence of future control signals $D_3(k), D_3(k+1) \ldots\ldots D_3(k+N-1)$, which makes the output voltage $\hat{V}(k+j)$ closest to the reference $V_0^{ref}(k+j)$ with the constraints on D_3 given in (17) defined using Table.1.

In MPC, a longer prediction horizon generally results in better control performance and stability of the converter. However, a longer prediction horizon also increases computational complexity as the number of computations grows exponentially with the length of the prediction horizon. Moreover, the optimization problem needs to solved at each time step whereas the time required to solve the MPC problem is much longer than the usual sampling interval used in power electronics converters, thus, long prediction horizons are not a feasible choice in real time implementation. Therefore, a prediction horizon of N=1 is generally used in modulator-based MPC schemes [11], [12], [18], and [20]. A relatively longer prediction horizon can be used in direct MPC schemes when the converter has less switches and can be manipulated directly without a modulation stage [9].

The system model presented in this paper is complex and requires modulation stages. Therefore, to reduce complexity and make the real time implementation possible the control problem presented is solved only for a prediction horizon, N=1. The optimal value of D_3 is given by (18).

$$D_3 = D_1 \pm \sqrt{D_1D_2 + \frac{4f^2LC(V_0 - V_0^{ref})}{V_{in}} - \frac{4i_0fL}{V_{in}}} \tag{18}$$

It is evident from (18) that value of the output phase shift D_3 depends on the error of the output voltage, which is the input to the predictive controller. There can be steady state error in the output voltage due to model mismatch and precision of micro-controller as discussed in [18] and [28]. This error can be compensated by introducing a correction factor into the input of the predictive controller. The correction factor is obtained from the output of the PI controller with the normalized difference of the output voltage and reference voltage as input [18] and [28]. However, there was no steady state error in the output voltage as presented in the result section while evaluating our proposed work both through simulations and experiments. Therefore, this study has not considered any correction factor in the design of proposed controller.

The constraints on D_3 mode-III are given by (17). If the calculated value is out of range, then the maximum value of

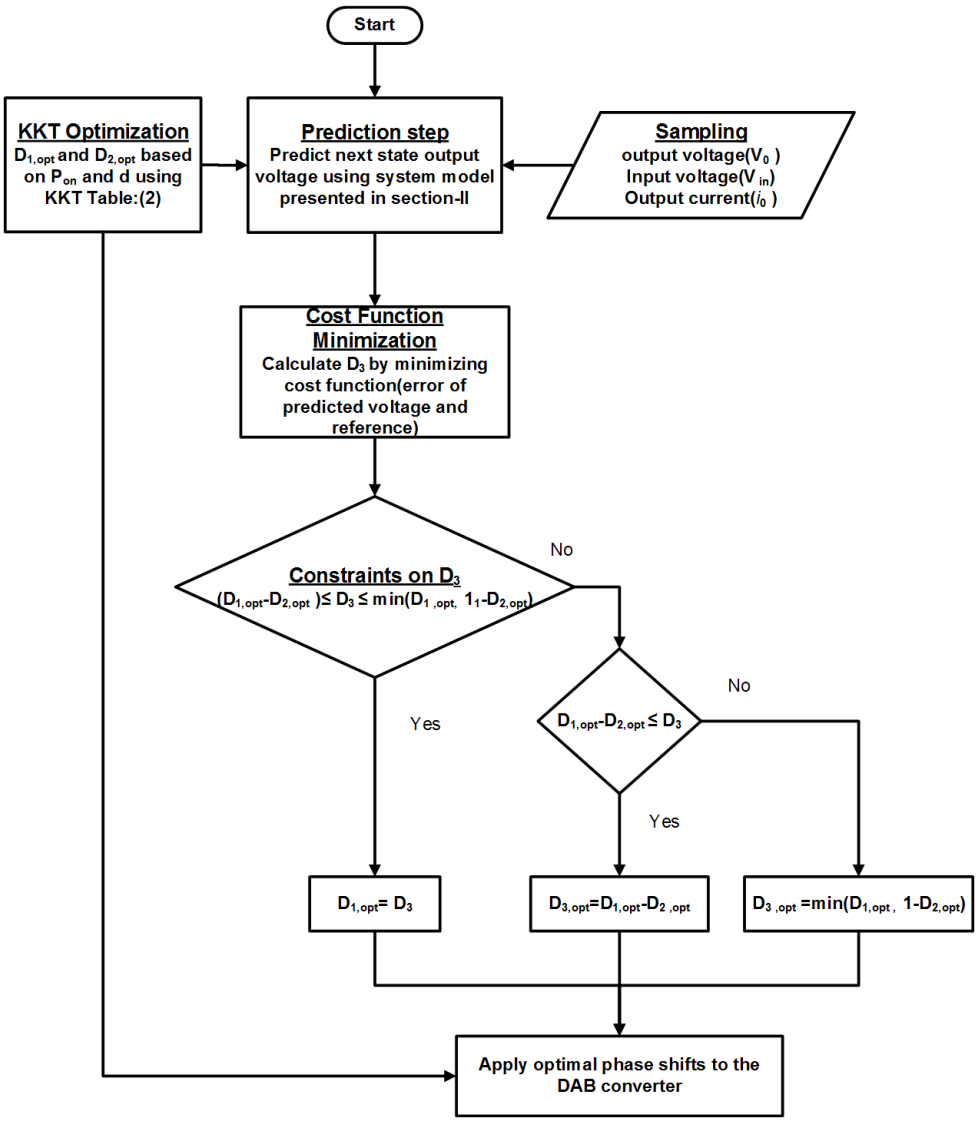

FIGURE 3. Flow diagram of proposed work.

D_3 as defined in (17) will be used. Hence, (18) can be used to find the optimal value of D_3 to improve the dynamic performance of dc-dc converter operating under TPS modulation.

The steps involved in the proposed algorithm are demonstrated using the flow diagram given in Fig.3. At the start of each switching period the next value of the output voltage is calculated using the prediction model presented in the previous section. The present values of input voltage, output voltage and output current as well as phase shifts D_1 and D_2 are required by the model at this step. The present states values are directly measured from the DAB circuit using the voltage and current sensors thus eliminating the need of observers [32], [35], and [36]. While equations derived using KKT optimizations are used to calculate the optimal values of phase shifts to limit the current stress. The next step is to find the value of D_3 by minimizing the cost function which consists of the error between the predicted output next state voltage and the reference. The subsequent step is to check and implement the constraints on D_3 to ensure that the converter is operating in mode-III which is the minimum current stress operating mode. Finally, the optimal values of the phase shifts are applied to converter, which ensure minimum current stress as well as fast transient response. Moreover, as mentioned in [25] that UTPS modulation strategy can achieve soft switching in the whole operating range, thus the augmentation of the proposed control algorithm with UTPS also results in soft switching.

The proposed control implementation to improve the dynamic performance of DAB dc-dc converter operating under TPS is also shown in the block diagram presented in Fig.4. $D_{1,opt}, D_{2,opt}, D_{3,opt}$ are the input parameters to the converter. The inner phase shifts $D_{1,opt}$ and $D_{2,opt}$ are calculated from the Table.2 presented in [25] using the KKT optimization. The KKT optimization needs P_{on} and d as inputs to calculate inner phase shifts. The predictive controller calculates the optimal value of outer phase shift $D_{3,opt}$

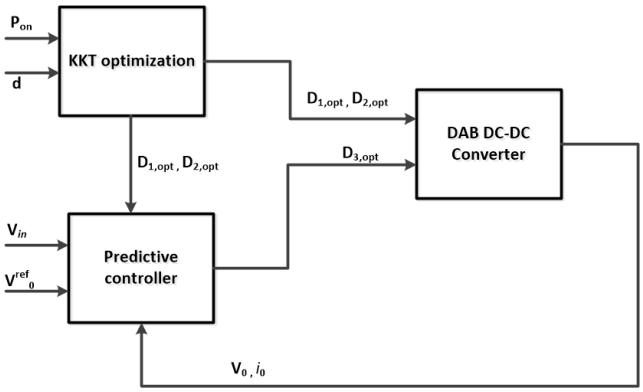

FIGURE 4. Block diagram showing proposed MPC based control.

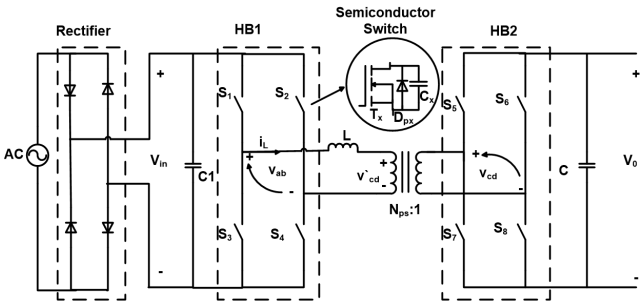

FIGURE 5. DAB DC-DC Converter with Input Voltage having ripple.

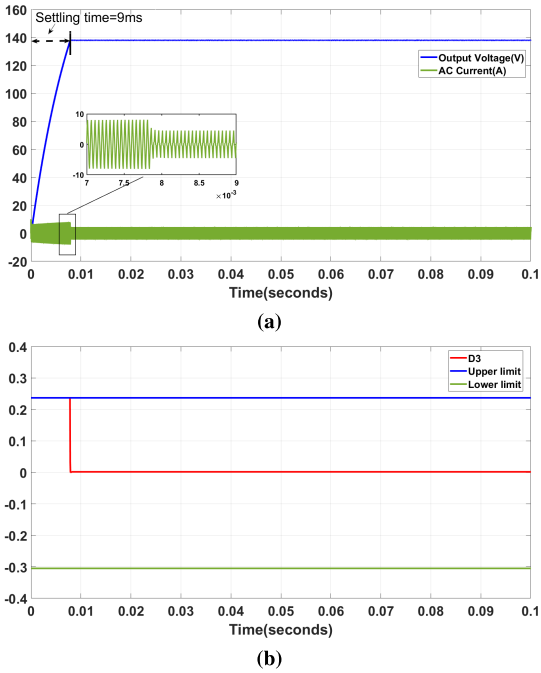

FIGURE 6. Start up process (a) Output Voltage and Inductor Current (b) $D_{3,opt}$.

using (18) using the sampled state values and optimal inner phase shift ratios.

V. SIMULATION RESULTS

To evaluate the proposed work, extensive simulations have been carried out using PLECS. The simulation parameters used for the DAB converter in this analysis are given in Table (3). Dynamic performance has been evaluated for mode-III.

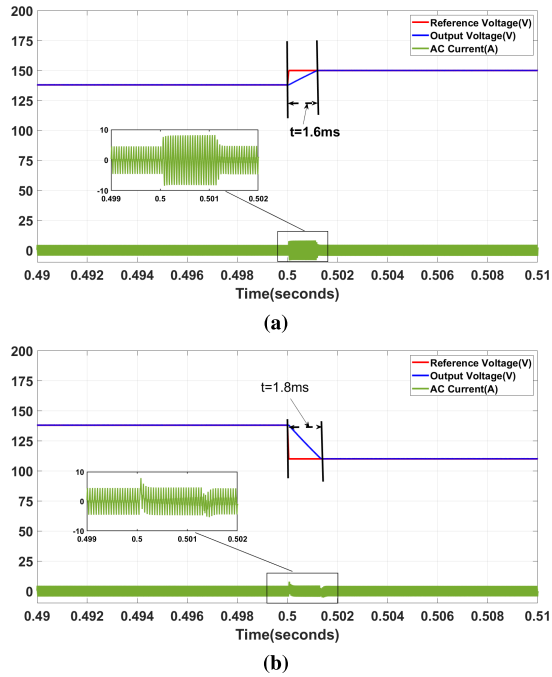

FIGURE 7. Dynamic response when output reference voltage (a) steps up from 138V to 150V (b) steps down from 138V to 110V.

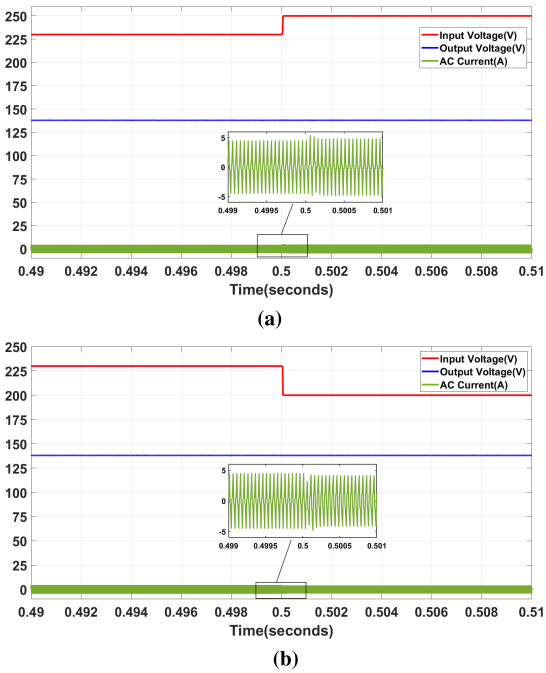

FIGURE 8. Dynamic response when input voltage (a) steps up from 230V to 250V (b) steps down from 230V to 200V.

A. START-UP PROCESS

The transient performance of the proposed control algorithm at the start-up for the converter with operating at nominal

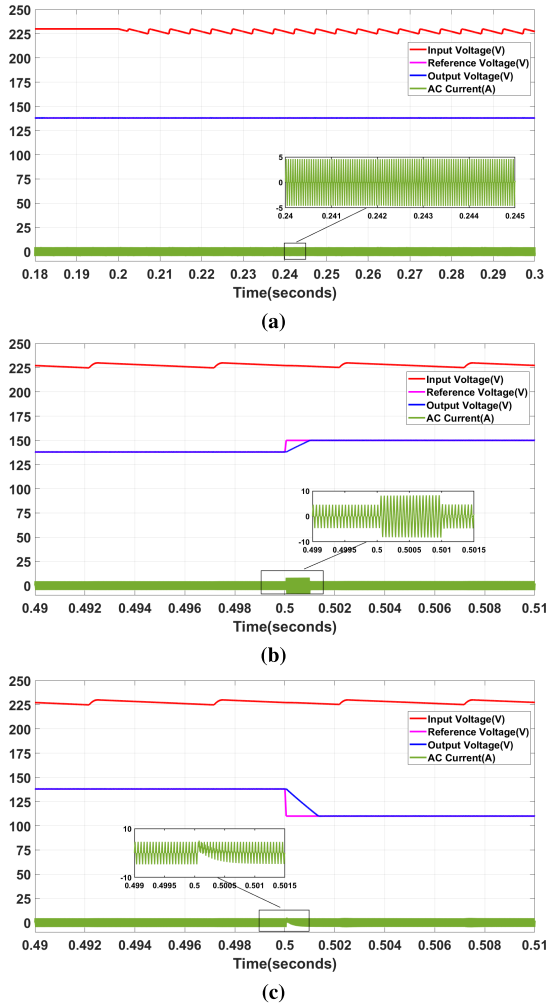

FIGURE 9. (a) input voltage containing ripple is applied at=0.2s (b) reference is stepped up from 138V to 150V at t=0.5s (c)reference is stepped down from 138V to 110V at t=0.5s.

TABLE 3. Simulation parameters of DAB DC-DC Converter.

Parameters	Symbol	Values
Input voltage	V_{in}	230 V
Reference output voltage	V_0^{ref}	138 V
Load resistance	R	77.69 Ω
Input Capacitance	C_1	480 μF
Output Capacitance	C	150 μ F
Inductance value	L	226.6 μ H
Transformer ratio	n	1:1
Switching frequency	f	20 kHZ

operating parameters given in the Table.3 has been presented in the Fig. 6. From Fig.6a the charging time of the output capacitor during start-up is 9ms with no overshoot. Fig.6b presents outer phase shift $D_{3,opt}$, it shows that $D_{3,opt}$ has a very large value at the start thus the steady state is achieved very quickly under MPC.

B. STEP CHANGES IN OUTPUT REFERENCE VOLTAGE

This subsection presents the performance of the proposed work when a step change is required in the voltage while

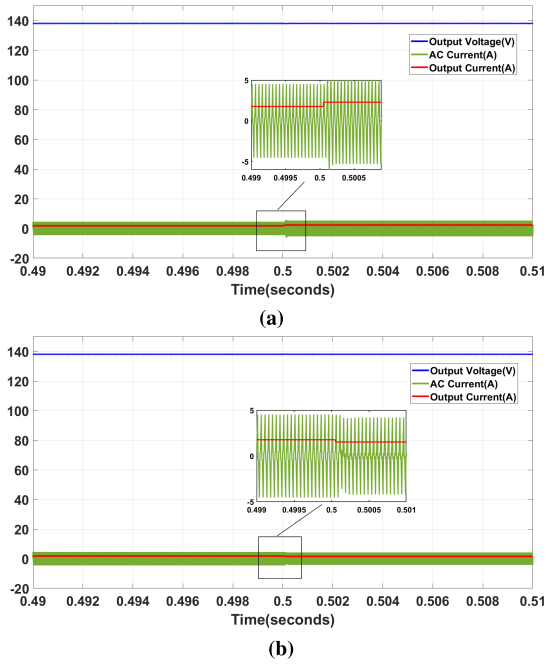

FIGURE 10. Dynamic response when load resistance (a) steps down from 77.69Ω to 50Ω (b) steps up from 77.69Ω to 90Ω.

TABLE 4. Hardware components.

Component	Description	Parameters
Switching devices	SKM75GB176D	$V_{CES} = 1700V$ $I_C = 80A$
Input Capacitors	C4DE	480 μF
Output Capacitors	IEC 61071 DownCap DTR	230 μ F 50 μ F
Magnetic components	Core ETD 59/31/22 N97 Litz Wire	$L_S = 226.6\mu$ H
Voltage sensors	LV 25-p	$t_r = 25\mu$S
Current sensors	LA 55-p	BW=25 μS 200kHz

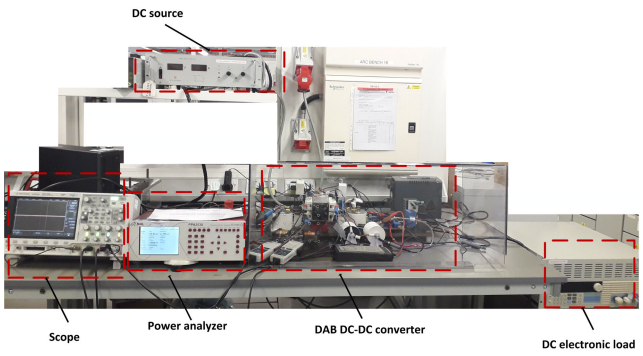

FIGURE 11. Experimental setup.

converter is operating at the nominal parameters given in Table. 3. The reference voltage V_0^{ref} is stepped up at t=0.5sec from 138V to 150V, when the converter has achieved steady state. Fig.7a shows that the time required to achieve the new reference value using MPC is 1.6ms. Fig.7b shows the transient results when the reference voltage V_0^{ref}

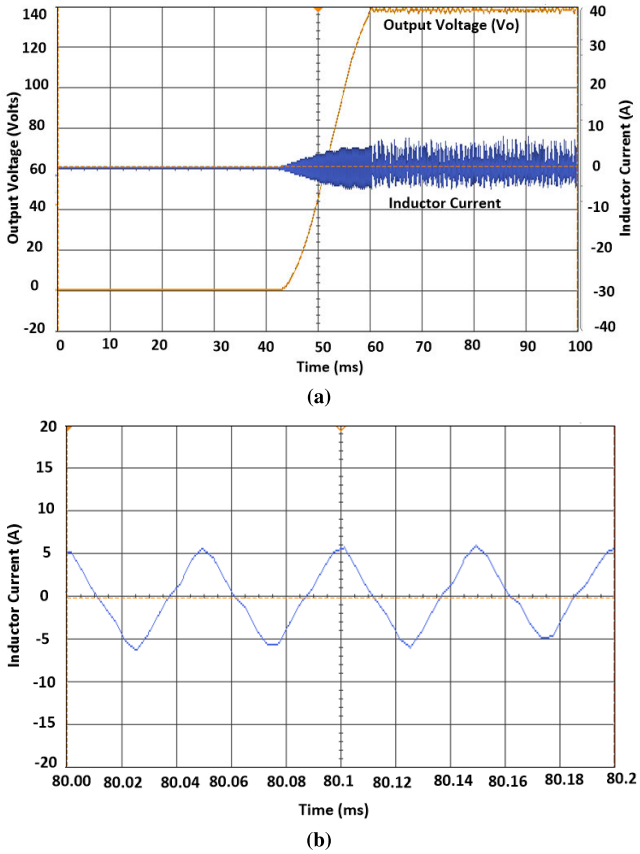

FIGURE 12. Dynamic response at start up(a) Output Voltage and Inductor Current (b) Inductor current.

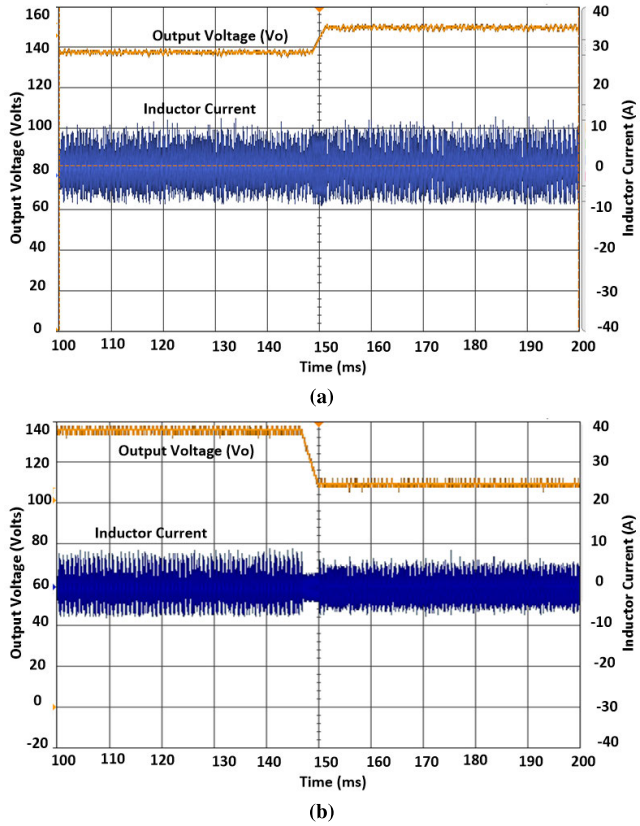

FIGURE 13. Dynamic response when output reference voltage (a) steps up from 138V to 150V (b) steps down from 138V to 110V.

is stepped down from 138V to 110V, the settling time that the MPC needs to achieve the new reference output voltage is 1.8ms.

C. STEP CHANGES IN INPUT VOLTAGE

The step changes the input voltage and its effect on the output voltage of the DAB converter is evaluated in this subsection. The input voltage is stepped up and down from the nominal value given in the Table. 3 while converter has achieved steady state. It is observed that the output voltage remains unchanged with MPC when the input voltage is stepped up from 230V to 250V and stepped down from 230V to 90V at t=0.5sec as shown in Fig.8a and Fig.8b, respectively.

D. RIPPLE IN INPUT VOLTAGE

This subsection presents the dynamic performance of the proposed control technique when the input source voltage includes ripple. To evaluate the performance under the ripple in the source voltage, the circuit used in the simulation is shown in Fig.5. The input is supplied by rectifying an ac source having peak value of 230V and 230Hz frequency. A bridge rectifier is used to convert ac to dc. Although a capacitor is used to smooth out the dc obtained from the rectifier, the low frequency ripples still exist after rectification.

For mode-III, the load is $R = 77.69\Omega$ and $V_0^{ref} = 138V$, Fig.9a shows the result when the input is switched at t=0.2s from a constant dc source to an input having a 5V peak-peak ripple. It shows that the output voltage is the same irrespective of the ripple content on the input voltage. Fig. 9b shows the transient performance when a step change is required in the reference voltage at t=0.5s. It shows that the controller is able to regulate the output voltage to the required reference value. Although the ripple in the input voltage have increased, the controller has the capability to reject the disturbances in the input voltage.

E. STEP CHANGES IN LOAD

The robustness of the proposed control algorithm to step changes in load is demonstrated in Fig.10. It is observed that the output voltage remains unchanged when the load resistance is stepped down from 77.69Ω to 50Ω and stepped up from 77.69Ω to 90Ω at t=0.5sec as shown in Fig.10a and 10b, respectively.

VI. EXPERIMENTAL RESULTS

The proposed control algorithm has been validated using a 1kW laboratory DAB prototype. The experimental prototype is shown in Fig. 11. Table 4 provides a list of the main components used in the design of the hardware. The hardware setup is adapted from [16], [19], and [32] with some modifications

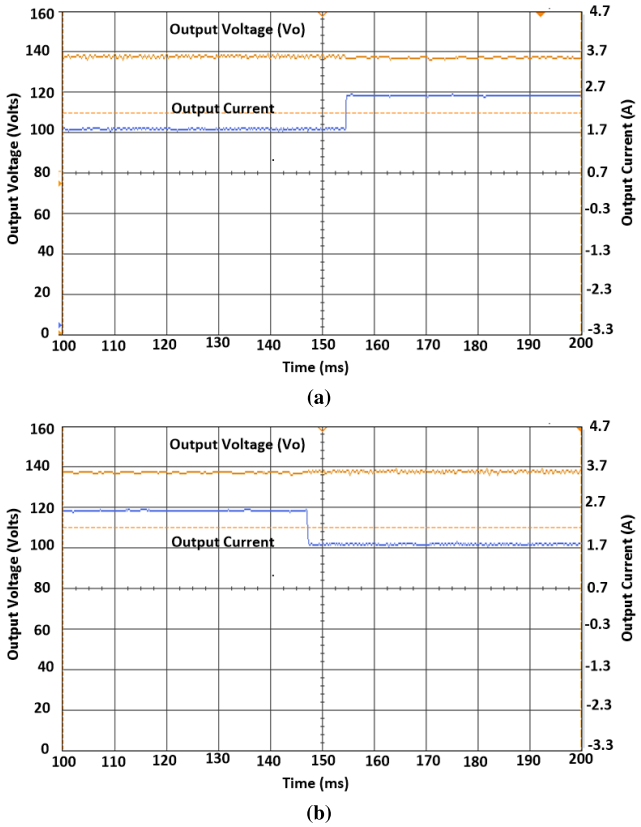

FIGURE 14. Dynamic response when load current (a) step up from 1.77A to 2.6A (b) step down from 2.6A to 1.77A.

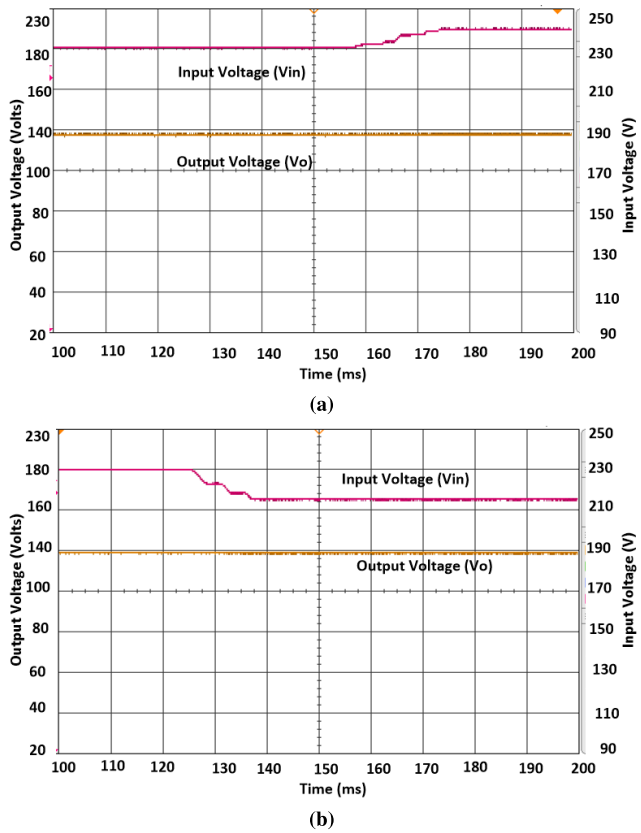

FIGURE 15. Dynamic response when input voltage (a) steps up from 230V to 240V (b) steps down from 240V to 215V.

to the transformer design. The series inductance consists of the leakage inductance of the transformer and a small external inductor to adjust the total inductance of the converter. The HBs are formed using IGBTs. A TMS320F2837xD evaluation board from Texas Instrument, which communicates with a host computer, has been used as the digital control platform.

A DC source is used as the input voltage, the nominal value of input voltage is 230V. A DC electronic load is used at the output of the converter. The DC electronic load can be operated in constant resistance mode or constant current mode. To evaluate the dynamic performance of the proposed control technique at the start up, the output reference voltage is set at $V_o^{ref} = 138V$ resulting in a conversion ratio of d=0.6. The electronic load is operated in the constant resistance mode by setting the load resistance equal to 77.69Ω. The dynamic performance at the startup is shown in Fig.12. The output voltage and inductor current are shown in the Fig. 12a with voltage scaling on left y-axis and inductor current scaling on right y-axis. Fig.12b shows the magnified waveform of the inductor current. The converter needs 15ms to reach a voltage of 138V at the output as set by the reference.

To check the response of the proposed control techniques to the changes in reference output voltage, a constant resistance equal to 77.69Ω is maintained at the output by operating the DC electronic load in constant resistance mode. The reference voltage is stepped up/down once the converter has reached steady state. Fig.13a depicts the response when the reference voltage is stepped up from 138V to 150V, while the converter is operating in steady state. As shown in the Fig.13a, 5ms are required by the control algorithm to adjust the output voltage of the converter to the new reference. Similarly, the reference voltage is stepped down to a new value of 110V. The dynamic performance is observed and shown in the Fig.13b.

To evaluate the dynamic performance of the proposed control technique under the variations in load, the DC electronic load is used in current mode. The output current is stepped up/down at the specified time instant while keeping the reference for the output voltage constant. Fig.14a shows the dynamic response when the load current steps up from 1.77A to 2.6A. Similarly, Fig. 14b presents the case when the load current is stepped down from 2.6A to 1.77A. It is observed that the output voltage remains constant irrespective of changes in the load.

Moreover, the robustness of the proposed control technique is also evaluated when there are fluctuations in the input voltage as shown in Fig.15. Fig.15a shown the effect on the output voltage when the input voltage has been changed from 230V to 240V. Similarly, Fig.15 presents the scenario when the input voltage is changed from 230V to 215V. These experimental results show that converter operating under the proposed control technique can reject disturbances generated as a result of variations in the input voltage

VII. CONCLUSION

In this paper, model predictive control with current stress optimization has been proposed to achieve fast dynamic response in a DAB dc-dc converter operating under triple phase shift modulation. A mathematical model has been developed to predict the next state value of the output voltage. A cost function has been defined considering the error between the predicted output voltage and the reference. Optimal values of the outer phase shift are calculated by minimizing the cost function. The proposed control technique has been evaluated at start-up and under the conditions resulting from the disturbances generated due to variations in load, fluctuations in input voltage and step changes in reference. Both the simulations and experimental results show that these disturbances are successfully rejected using this technique.

REFERENCES

[1] R. W. A. A. De Doncker, D. M. Divan, and M. H. Kheraluwala, "A three-phase soft-switched high-power-density DC/DC converter for high-power applications," *IEEE Trans. Ind. Appl.*, vol. 27, no. 1, pp. 63–73, Jan./Feb. 1991, doi: 10.1109/28.67533.

[2] N. G. Hingorani, *Understanding FACTs: Concept and Technology of Flexible AC Transmission Systems*. Piscataway, NJ, USA: IEEE Press, 2000.

[3] Z. Chen, J. M. Guerrero, and F. Blaabjerg, "A review of the state of the art of power electronics for wind turbines," *IEEE Trans. Power Electron.*, vol. 24, no. 8, pp. 1859–1875, Aug. 2009, doi: 10.1109/TPEL.2009.2017082.

[4] J. M. Carrasco, L. G. Franquelo, J. T. Bialasiewicz, E. Galván, R. C. PortilloGuisado, M. A. M. Prats, J. I. León, and N. Moreno-Alfonso, "Power-electronic systems for the grid integration of renewable energy sources: A survey," *IEEE Trans. Ind. Electron.*, vol. 53, no. 4, pp. 1002–1016, Jun. 2006, doi: 10.1109/TIE.2006.878356.

[5] S. Bifaretti, P. Zanchetta, A. Watson, L. Tarisciotti, and J. C. Clare, "Advanced power electronic conversion and control system for universal and flexible power management," *IEEE Trans. Smart Grid*, vol. 2, no. 2, pp. 231–243, Jun. 2011, doi: 10.1109/TSG.2011.2115260.

[6] T. Zhao, L. Yang, J. Wang, and A. Q. Huang, "270 kVA solid state transformer based on 10 kV SiC power devices," in *Proc. IEEE Electr. Ship Technol. Symp.*, May 2007, pp. 145–149, doi: 10.1109/ESTS.2007.372077.

[7] J. H. Lee, "Model predictive control: Review of the three decades of development," *Int. J. Control, Autom. Syst.*, vol. 9, no. 3, pp. 415–424, Jun. 2011, doi: 10.1007/s12555-011-0300-6.

[8] S. Kouro, P. Cortés, R. Vargas, U. Ammann, and J. Rodríguez, "Model predictive control—A simple and powerful method to control power converters," *IEEE Trans. Ind. Electron.*, vol. 56, no. 6, pp. 1826–1838, Jun. 2009, doi: 10.1109/TIE.2008.2008349.

[9] P. Karamanakos, T. Geyer, and S. Manias, "Direct voltage control of DC–DC boost converters using enumeration-based model predictive control," *IEEE Trans. Power Electron.*, vol. 29, no. 2, pp. 968–978, Feb. 2014, doi: 10.1109/TPEL.2013.2256370.

[10] S. Vazquez, J. Rodriguez, M. Rivera, L. G. Franquelo, and M. Norambuena, "Model predictive control for power converters and drives: Advances and trends," *IEEE Trans. Ind. Electron.*, vol. 64, no. 2, pp. 935–947, Feb. 2017, doi: 10.1109/TIE.2016.2625238.

[11] Z. Song, Y. Tian, W. Chen, Z. Zou, and Z. Chen, "Predictive duty cycle control of three-phase active-front-end rectifiers," *IEEE Trans. Power Electron.*, vol. 31, no. 1, pp. 698–710, Jan. 2016, doi: 10.1109/TPEL.2015.2398872.

[12] R. Vargas, U. Ammann, J. Rodriguez, and J. Pontt, "Predictive strategy to control common-mode voltage in loads fed by matrix converters," *IEEE Trans. Ind. Electron.*, vol. 55, no. 12, pp. 4372–4380, Dec. 2008, doi: 10.1109/TIE.2008.2007016.

[13] K. Antoniewicz, M. Jasinski, M. P. Kazmierkowski, and M. Malinowski, "Model predictive control for three-level four-leg flying capacitor converter operating as shunt active power filter," *IEEE Trans. Ind. Electron.*, vol. 63, no. 8, pp. 5255–5262, Aug. 2016, doi: 10.1109/TIE.2016.2536584.

[14] J. Rodriguez, J. Pontt, C. A. Silva, P. Correa, P. Lezana, P. Cortes, and U. Ammann, "Predictive current control of a voltage source inverter," in *IEEE Trans. Ind. Electron.*, vol. 54, no. 1, pp. 495–503, Feb. 2007, doi: 10.1109/TIE.2006.888802.

[15] F. Kieferndorf, P. Karamanakos, P. Bader, N. Oikonomou, and T. Geyer, "Model predictive control of the internal voltages of a five-level active neutral point clamped converter," in *Proc. IEEE Energy Convers. Congr. Expo. (ECCE)*, Sep. 2012, pp. 1676–1683, doi: 10.1109/ECCE.2012.6342611.

[16] Q. Xiao, L. Chen, H. Jia, P. W. Wheeler, and T. Dragičević, "Model predictive control for dual active bridge in naval DC microgrids supplying pulsed power loads featuring fast transition and online transformer current minimization," *IEEE Trans. Ind. Electron.*, vol. 67, no. 6, pp. 5197–5203, Jun. 2020, doi: 10.1109/TIE.2019.2934070.

[17] Y. Xie, R. Ghaemi, J. Sun, and J. S. Freudenberg, "Model predictive control for a full bridge DC/DC converter," *IEEE Trans. Control Syst. Technol.*, vol. 20, no. 1, pp. 164–172, Jan. 2012, doi: 10.1109/TCST.2011.2107575.

[18] F. An, W. Song, B. Yu, and K. Yang, "Model predictive control with power self-balancing of the output parallel DAB DC–DC converters in power electronic traction transformer," *IEEE J. Emerg. Sel. Topics Power Electron.*, vol. 6, no. 4, pp. 1806–1818, Dec. 2018, doi: 10.1109/JESTPE.2018.2823364.

[19] L. Chen, S. Shao, Q. Xiao, L. Tarisciotti, T. Dragicevic, and P. Wheeler, "Model predictive control for dual-active-bridge converters supplying pulsed power loads in naval DC micro-grids," *IEEE Trans. Power Electron.*, vol. 35, no. 2, pp. 1957–1966, Feb. 2020, doi: 10.1109/TPEL.2019.2917450.

[20] D. Qin, Q. Sun, D. Ma, and J. Sun, "Model predictive control of dual-active-bridge based fast battery charger for plug-in hybrid electric vehicle in the future grid," in *Proc. IEEE Innov. Smart Grid Technol.-Asia (ISGT Asia)*, Chengdu, China, May 2019, pp. 277.692–277.696, doi: 10.1109/ISGT-Asia.2019.8881457.

[21] F. Krismer and J. W. Kolar, "Closed form solution for minimum conduction loss modulation of DAB converters," *IEEE Trans. Power Electron.*, vol. 27, no. 1, pp. 174–188, Jan. 2012, doi: 10.1109/TPEL.2011.2157976.

[22] J. Everts, F. Krismer, J. Van den Keybus, J. Driesen, and J. W. Kolar, "Optimal ZVS modulation of single-phase single-stage bidirectional DAB AC–DC converters," *IEEE Trans. Power Electron.*, vol. 29, no. 8, pp. 3954–3970, Aug. 2014, doi: 10.1109/TPEL.2013.2292026.

[23] J. Everts, "Closed-form solution for efficient ZVS modulation of DAB converters," *IEEE Trans. Power Electron.*, vol. 32, no. 10, pp. 7561–7576, Oct. 2017, doi: 10.1109/TPEL.2016.2633507.

[24] A. Tong, L. Hang, and G. Li, "Optimized control strategy for minimum ohmic loss of dual active bridge converter," in *Proc. IEEE Appl. Power Electron. Conf. Expo. (APEC)*, Mar. 2017, pp. 1103–1110, doi: 10.1109/APEC.2017.7930833.

[25] J. Huang, Y. Wang, Z. Li, and W. Lei, "Unified triple-phase-shift control to minimize current stress and achieve full soft-switching of isolated bidirectional DC–DC converter," *IEEE Trans. Ind. Electron.*, vol. 63, no. 7, pp. 4169–4179, Jul. 2016, doi: 10.1109/TIE.2016.2543182.

[26] C. Mi, H. Bai, C. Wang, and S. Gargies, "Operation, design and control of dual H-bridge-based isolated bidirectional DC–DC converter," *IET Power Electron.*, vol. 1, no. 4, pp. 507–517, Dec. 2008, doi: 10.1049/iet-pel:20080004.

[27] J. Rodrigreuz and P. Cortes, *Predictive Control of Power Converters and Electrical Drives*. Hoboken, NJ, USA: Wiley, Apr. 2012.

[28] S. Dutta, S. Hazra, and S. Bhattacharya, "A digital predictive current-mode controller for a single-phase high-frequency transformer-isolated dual-active bridge DC-to-DC converter," *IEEE Trans. Ind. Electron.*, vol. 63, no. 9, pp. 5943–5952, Sep. 2016, doi: 10.1109/TIE.2016.2551201.

[29] S. Shao, H. Chen, X. Wu, J. Zhang, and K. Sheng, "Circulating current and ZVS-on of a dual active bridge DC–DC converter: A review," *IEEE Access*, vol. 7, pp. 50561–50572, 2019, doi: 10.1109/ACCESS.2019.2911009.

[30] B. Wang, V. R. K. Kanamarlapudi, L. Xian, X. Peng, K. T. Tan, and P. L. So, "Model predictive voltage control for single-inductor multiple-output DC–DC converter with reduced cross regulation," *IEEE Trans. Ind. Electron.*, vol. 63, no. 7, pp. 4187–4197, Jul. 2016, doi: 10.1109/TIE.2016.2532846.

[31] F. M. Oettmeier, J. Neely, S. Pekarek, R. DeCarlo, and K. Uthaichana, "MPC of switching in a boost converter using a hybrid state model with a sliding mode observer," *IEEE Trans. Ind. Electron.*, vol. 56, no. 9, pp. 3453–3466, Sep. 2009, doi: 10.1109/TIE.2008.2006951.

[32] L. Chen, L. Lin, S. Shao, F. Gao, Z. Wang, P. W. Wheeler, and T. Dragicevic, "Moving discretized control set model-predictive control for dual-active bridge with the triple-phase shift," *IEEE Trans. Power Electron.*, vol. 35, no. 8, pp. 8624–8637, Aug. 2020, doi: 10.1109/TPEL.2019.2962838.

[33] Y. Xie, R. Ghaemi, J. Sun, and J. S. Freudenberg, "Implicit model predictive control of a full bridge DC–DC converter," *IEEE Trans. Power Electron.*, vol. 24, no. 12, pp. 2704–2713, Dec. 2009, doi: 10.1109/TPEL.2009.2030196.

[34] R. Baidya, R. P. Aguilera, P. Acuna, T. Geyer, R. A. Delgado, D. E. Quevedo, and H. D. T. Mouton, "Enabling multistep model predictive control for transient operation of power converters," *IEEE Open J. Ind. Electron. Soc.*, vol. 1, pp. 284–297, 2020, doi: 10.1109/OJIES.2020.3029358.

[35] T. Dorfling, H. du Toit Mouton, T. Geyer, and P. Karamanakos, "Long-horizon finite-control-set model predictive control with nonrecursive sphere decoding on an FPGA," *IEEE Trans. Power Electron.*, vol. 35, no. 7, pp. 7520–7531, Jul. 2020, doi: 10.1109/TPEL.2019.2956213.

[36] M. Vatani, B. Bahrani, M. Saeedifard, and M. Hovd, "Indirect finite control set model predictive control of modular multilevel converters," *IEEE Trans. Smart Grid*, vol. 6, no. 3, pp. 1520–1529, May 2015, doi: 10.1109/TSG.2014.2377112.

[37] K. Areerak, S. V. Bozhko, L. De Lillo, G. M. Asher, D. W. P. Thomas, A. Watson, and T. Wu, "The stability analysis of AC–DC systems including actuator dynamics for aircraft power systems," in *Proc. 13th Eur. Conf. Power Electron. Appl.*, 2009, pp. 1–10.

SEEMA MIR AKBAR received the master's degree in electrical engineering from the National University of Sciences and Technology, Islamabad, Pakistan, in 2016, where she is currently pursuing the Ph.D. degree in electrical engineering. Since October 2019, she has been a Visiting Research Scholar with the Power Electronics Machines and Control Group, University of Nottingham. Her current research interests include model predictive control and optimization of power electronic converters.

AMMAR HASAN was born in Pakistan, in 1982. He received the B.E. degree in electrical engineering from the National University of Sciences and Technology, Islamabad, Pakistan, in 2004, and the master's and Ph.D. degrees in control systems from the Imperial College London, London, U.K., in 2008 and 2012, respectively.

Since 2012, he has been with the School of Electrical Engineering and Computer Science, National University of Sciences and Technology, where he is currently an Associate Professor. His current research interests include model predictive control, control of power electronic converters, optimization techniques for control systems, and numerical algorithms as dynamical systems.

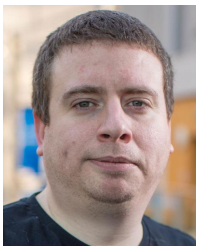

ALAN J. WATSON (Senior Member, IEEE) received the M.Eng. (Hons.) and Ph.D. degrees in electronic engineering from the University of Nottingham, U.K., in 2004 and 2008, respectively. In 2009, he became a Research Fellow with the Power Electronics Machines and Control Group, University of Nottingham. Since 2009, he has been involved in various projects in the area of high-power electronics, including resonant converters, high-voltage power supplies, and multilevel converters for grid connected applications, such as HVDC and flexible ac transmission systems. In 2012, he was promoted to a Senior Research Fellow before becoming an Assistant Professor in high power electronics with the University of Nottingham, in 2013. His current research interests include the development and control of advanced high-power conversion topologies for industrial applications, grid connected converters, and HVDC transmission.

PAT WHEELER (Fellow, IEEE) received the B.Eng. (Hons.) and Ph.D. degrees in electrical engineering for his work on matrix converters from the University of Bristol, U.K., in 1990 and 1994, respectively. In 1993, he moved to the University of Nottingham, U.K., and worked as a Research Assistant with the Department of Electrical and Electronic Engineering. In 1996, he became a Lecturer with the Power Electronics, Machines and Control Group, University of Nottingham, where he has been a Full Professor, since January 2008. He was the Head of the Department of Electrical and Electronic Engineering, University of Nottingham, from 2015 to 2018. He is currently the Head of the Power Electronics, Machines and Control Research Group and the Global Director of the Institute of Aerosapce Technology, University of Nottingham. He was the Li Dak Sum Chair Professor in electrical and aerospace engineering. He has published over 750 academic publications in leading international conferences and journals. He is a member of the IEEE PELs AdCom and is currently the IEEE PELS Vice-President for Technical Operations.